# Exploration the mechanism of doxorubicin-induced Heart failure in Rats by integration of proteomics and metabolomics data

**Yu Yuan**
Tianjin University of Traditional Chinese Medicine
**Simiao Fan**
Tianjin University of Traditional Chinese Medicine
**Lexin Shu**
Tianjin University of Traditional Chinese Medicine
**Wei Huang**
Tianjin University of Traditional Chinese Medicine
**Lijuan Xie**
Tianjin University of Traditional Chinese Medicine
**Chenghao Bi**
Tianjin University of Traditional Chinese Medicine
**Hongxin Yu**
Tianjin University of Traditional Chinese Medicine
**Yuming Wang** ( wangyuming226@163.com )
Tianjin University of Traditional Chinese Medicine
**Yubo Li** ( yaowufenxi001@sina.com )
Tianjin University of Traditional Chinese Medicine https://orcid.org/0000-0003-0455-0969

**Research article**

**Keywords:** Doxorubicin, Heart failure, Proteomics, Metabonomics, PTP1B

**Posted Date:** August 19th, 2020

**DOI:** https://doi.org/10.21203/rs.3.rs-58887/v1

## Abstract

# Background

Heart failure is currently a worldwide systemic disease with high morbidity and mortality and is very common. At present, many studies have shown that heart failure is associated with obesity, hypertension and diabetes, but it is still unable to prevent the disease from progressing. Here, we elucidate the molecular mechanisms of doxorubicin–induced harmful effects on rat cardiac metabolism and function from a new perspective, using metabonomics and Proteomics analysis data.

# Methods

The aim of this study was to use metabonomic and proteomic techniques to systematically elucidate the molecular mechanisms of doxorubicin (DOX)–induced heart failure (HF) in rat. In this study, we aimed to systematically elucidate the molecular action of Dox on rats heart and the reasons for DOX–induced the HF mechanism through the metabonomics tandem mass tag (TMT)–based quantitative proteomics approach. Rats were gavaged with DOX (3 mg/kg) for 6 weeks and the plasma metabonomics, cardiac tissue proteomics, histopathology and related proteins expression levels.

# Results

A total of 278 proteins and 21 metabolites were significantly altered in rats following DOX treatments. The responsive proteins and metabolites were predominantly involved in Fatty acid metabolism, Glycolysis, glycerophospholipid metabolism, TCA cycle, Glutathione metabolism, Myocardial contraction.

# Conclusions

The present study indicates the PTP1B inhibits the expression of HIF-1α by inhibiting the phosphorylation of IRS, leading to disorders of fatty acid metabolism and glycolysis, which together with the decrease of Nrf2, SOD, Cytc and AK4 proteins lead to oxidative stress, suggesting the PTP1B may serve as a potential target in the treatment of heart failure.

## Introduction

Heart failure, as a syndrome of the ultimate pathway of most cardiovascular systems, can affect a wide range of people in all ages(Sliwa, 2020). Abnormal cardiac structure or function, dysfunction of systolic function and/or diastolic function, and reduction of ventricular ejection volume will lead to cardiac circulatory disorders(Eisenberg et al., 2018; Maurer and Packer, 2020), which can cause cardiac fibrillation, arrhythmia, heart failure and other diseases. At the same time, many studies have proved that there is a significant sexual relationship between heart failure and hypertension, kidney disease,

coronavirus disease 2019 and obesity(Bangalore et al., 2020; Chen et al., 2020b; Rayner et al., 2020; Sliwa, 2020). Therefore, heart failure is currently a very common systemic disease in the world, with high morbidity and mortality. Currently, there are many studies on the therapeutic targets for heart failure, but it can not completely prevent the progression of the disease, for example, Cyclic nucleotide phosphodiesterase, apolipoprotein M, s-nitroso ation, etc., are closely related to anti-inflammatory, regulating cardiac hypertrophy and myocardial cell function, cardiac remodeling and dysfunction(Chen et al., 2020a; Chirinos et al., 2020; Tang et al., 2020). The discovery of these targets is helpful for the treatment of heart failure, but due to the complexity of heart failure, finding new targets will help heart failure to provide new strategies for effective treatment of diseases, finding new targets is helpful to provide new strategies for the effective treatment of heart failure (HF), the research and development of new drugs, and the study of the pharmacodynamic material basis.

In medicine, proteomics and metabonomics are used to help identify patients at risk of disease, detect and identify various molecules at the level of proteins and metabolites, and study their functions and interrelationships among various molecules(Mato et al., 2014). With the development of proteomics technology, tandem mass tag (TMT) labeling quantitative proteomics technology, as a novel quantitative method, can be used to quickly and quantitatively evaluate protein localization independent of antibody(Sueki et al., 2020). Based on proteomics of mass spectrometry has excellent analytical functions and is very suitable for basic research and clinical diagnosis of human diseases(Cifani and Kentsis, 2017). Metabolites control the expression of genes and proteins to a large extent, and drive key covalent chemical modifications of DNA and RNA (such as methylation) and proteins (post-translational modification), thereby affecting cell function(Rinschen et al., 2019). The combination of proteomics and metabonomic analysis can link genotypes and phenotypes to help determine the causal mechanism of heart failure(Hoffman et al., 2017).

To explore the mechanism of the HF pathogenesis, we used ultra–high performance liquid chromatography tandem quadrupole time–of–flight mass spectrometry (UPLC–Q–TOF/MS) to explain the toxicological pathways of doxorubicin on the heart, especially the combined proteomics technology, which provides more abundant information at the protein level. The combined use of proteomic and metabolomic analysis can help identify causal mechanisms of heart failure.

# Materials And Methods

### Chemicals

Doxorubicin (Solarbio, Beijing, China), Formaldehyde (Solarbio, Beijing, China), Heparin sodium (Solarbio, Beijing, China), Acetonitrile (Merck, Germany), Formic acid (CNW, Germany), BCA Kit (Solarbio, Shangahi, China), Tris (Sigma, U.S.A.), SDS (Bio–Rad, U.S.A.), Phenylmethylsulfonyl fluoride (Solarbio, Beijing), Phosphatase inhibitor (Solarbio, Beijing, China), RIPA buffer (Solarbio, Beijing, China), IRS–1, P–IRS, HK2, HIF–1α (Cell Signaling Technology, Inc., USA), Nrf2 (Abcam, U.S.A.), $NH_4HCO_3$ (Sigma, U.S.A.), High pH

Reversed–Phase Peptide Fractionation Kit (Pierce, U.S.A), TMT 6/10 plex Isobaric Label Reagent (Thermo, U.S.A.).

## Animals

A total of 35 male Wistar rats (180–200 g) were purchased from Beijing Weitong Lihua Experimental Animal Technology Co., Ltd., license number: SCXK (Beijing) 2016–0006. After one week of adaptive feeding, the rats were acclimatized to a 12–hour light/dark cycle in a controlled environment with a temperature of approximately 23 ± 2 °C and a relative humidity of 35 ± 5%. All animals recieved care and raising with standard food and tap water. The rats were randomly divided into a treatment group (Dox) and a control group (NS). The Dox group was injected intraperitoneally with doxorubicin (3 mg/kg) once a week, and the NS group was injected with the same amount of normal saline intraperitoneally, for 6 weeks.

## Compliance with ethical standards

This study was approved by the Institutional Animal Care and Use Committee of Tianjin University of Traditional Chinese Medicine (IACUC), and was conducted in accordance to the guidelines of the National Institutes of Health Animal Care and Use Committee.

## Biochemical and pathological observatio

After induction of anesthesia with 5% Chloral hydrate, the long–axis parasternal sections of rats were measured using an ultrasound Doppler instrument, and cardiac function indexes were recorded. Ejection fraction (EF) was used as a parameter to determine the establishment of heart failure. From each serum sample, 100 μL was extracted and measured in a Fully Automated Biochemical Instrument, the data of lactate dehydrogenase (LDH), troponin kinase (CK) and creatine kinase isoenzymes (CK–MB) were recorded.

A small section of heart tissues of NS and DOX were fixed with 10% formaldehyde, embedded in paraffin and then prepared into 5 μm–thick sections. Hematoxylin and eosin (H&E) staining was performed in heart sections to visulize the Pathological manifestations under the microscope.

## Metabolomics analysis

Metabonomics was studied from the serum of NS group and doxorubicin treated rats respectively. Plasma samples of rats were centrifuged at 4 °C and 3500 rpm for 10 min. Each sample was fed with 100 μL of serum, added 300 μL acetonitrile (1:3 volume ratio), and vortex 1 min. Ice water bath ultrasonic 10 min, in the freezing centrifuge (ALLLEGRATM–64R; American) in 13000 rmp, 4 °C centrifugation 15 min, retain supernatant. QC samples were prepared to make QC samples contain biological information of all samples.

To further assess unravel the alterations of metabolites in rats treated with doxorubicin, endogenous metabolites were analyzed by Waters Acquity UPLC coupled with Q–TOF/MS (Waters, Milford, MA, U.S.A.). 10 μL of sample solution was injected onto an Acquity UPLC BEH $C_{18}$ column (2.1 mm × 100 mm, 1.7 μm, Waters, U.S.A.) at 45 °C and the flow rate was 0.3 mL/min. The optimal mobile phase consisted of a linear gradient system of (A) 0.1% formic acid in water and (B) 0.1% formic acid in acetonitrile, 0–8.5 min, 1–25% B; 8.5–11.0 min, 25–50% B; 11.0–13.0 min, 50–1% B; 13.0–15.0 min, 1–1% B. In addition, the QC samples were contained most information of whole plasma samples.

The mass spectrum optimal conditions of analysis were as follow: Electrospray ionization (ESI) source was used, in positive and negative ionization modes, the capillary voltage was 3.0 kV, drying gas temperature was set at 325 °C, drying gas flow was 10 mL/min, desolvation gas flow was 600 L/h, source temperature was 120 °C, desolvation temperature was 350 °C and cone gas flow was 50 L/h. The quadrupole scan range was set at m/z 50–1000 Da.

### Quantitative proteomics analysis

Rat myocardial tissue samples were frozen with liquid nitrogen, ground and crushed with SDT lysate (4% SDS, 100 mM Tris–HCl, 1 mM DTT, pH 7.6 ) in MP homogenizer. Protein quantification was performed by BCA method. Each sample was taken 30 ml protein solution, enzymatically hydrolyzed by filter aidedp roteome preparation (FASP) method(Marwick, 2015), and the peptide segment was quantified under OD280. Each sample was labeled according to the instructions of Thermo TMT labeling kit. The labeled samples were combined and subjected to fractionation (See supplementary document 1 for detailed treatment).

Then each fraction was injected for HPLC analysis, followed by LC–MS/MS analysis performed on a Q Exactive mass spectrometer (Thermo Scientific) that was coupled to Easy nLC (Thermo Fisher Scientific). Buffer A is 0.1% formic acid buffer; B is 84% acetonitrile and 0.1% formic acid aqueous solution. The chromatographic columns used were packed with nanoViper $C_{18}$ (Thermo Scientific Acclaim PepMap100, 100 μm×2 cm, 3 μm, 100 A) balanced by 95% A solution at a flow rate of 300 nL/min. The peptides were eluted using a linear gradient (0–80 min, 0–55% B; 80–85 min, 55–100% B; 85–90 min, 100% B).

The detection mode is positive ion, the scanning range of parent ion is 300–1800 m/z, the resolution of primary mass spectrometry is 70,000 at 200 m/z, the target of Automatic Gain Control is 1e6, Maximum IT is 50 ms, and the Dynamic Exclusion time is 60.0 s. The mass–charge ratio of peptides and peptide fragments is collected according to the following methods: 20 fragment spectra ($MS^2$ scan) were collected after each full scan, $MS^2$ Activation Type was HCD, isolation window was 2 m/z, secondary mass spectrometry resolution was 17,500 at 200 m/z (TMT 6–plex) or 35,000 at 200 m/z (TMT 10–plex), 30 eV for Normalized Collision Energy and 0.1% for Underfill.

### Data processing

MassLynx software (Waters, Version 4.1) was used to extract peak values and correct the original mass spectra data of metabonomics for principal component analysis (PCA) and partial least squares–discriminant analysis (PLS–DA). The standard were variable importance in the projection (VIP) > 1.5 and T–test ($p < 0.05$) to select potential biomarkers. Subsequently according to the HMDB database (http://www.hmdb.ca), and the differential metabolites were further identification by m/z values and Mass Spectrometry Fragmentation. The identified metabolites were analyzed by receiver operating characteristic curve (ROC) and clustering analysis software was used according to the relative content of each biomarker (http://www.metaboanalyst.ca/) generate a heat map to evaluate the diagnostic ability of metabolic markers. Pathway and visualization analysis using the KEGG pathway database (http://mirror.MetaboAnalyst.ca/).

For the tandem mass tag (TMT) proteomic data, MS/MS spectra were searched using MASCOT engine (Matrix Science, London, UK, version 2.2) embedded into Proteome Discoverer 1.4 (supplementary 1). LC/MS raw data were searched in the UniProt–reviewed rat protein database and differentially expressed proteins were screened by the criteria of up–regulation greater than 1.2 times or down–regulation less than 0.83 and *p* value less than 0.05. All identified proteins were annotated with Blast2GO for GO function, and then differentially expressed proteins were analyzed by Fisher's exact test for GO functional enrichment and bioinformatics. Next, through the KEGG (http://www.kegg.jp/) pathway enrichment analysis of significantly differentially expressed proteins, we can help us to understand the metabolic or signal pathways that these proteins may be involved in.

### Western blot analysis

The 50 mg heart tissue was added to the phenylmethylsulfonyl fluoride (PMSF), phosphatase inhibitor and RIPA buffer, and lysed and cracked for 30 min on the ice to ensure complete cleavage. The protein was quantified with the BCA protein assay kit and then protein was separated by 8% SDS–PAGE. The proteins were transferred to polyvinylidene difluoride (PVDF) membrane and incubated overnight with primary antibodies against IRS–1, P–IRS, HK2, HIF–1 α, Nrf2, followed by incubation with β–actin and NADPH, which served as an internal control.

### Statistical analysis

The analysis of related data was performed using SPSS software (version 17.0). The experimental data are expressed as the mean ± SD. Data comparison between various experimental groups was performed by T–test or one–way ANOVA. $*p < 0.05$, $**p < 0.01$.

## Results

### Effect of doxorubicin on heart Biochemical parameters and Pathological Situations of rat

Doxorubicin is an effective cancer chemotherapy agent, which can cause pathological and physiological HF(Fu et al., 2016). Echocardiography directly reflected the ejection capacity, systolic and diastolic

function of the heart, and played an irreplaceable role in the diagnosis of cardiotoxicity. We compared the echocardiograms, A significant elevation of plasma diastolic left ventricular volume (LVID,d) and systolic left ventricular volume (LVID,s) were observed in DOX group compared with NS group over the entire time course, whereas the levels of EF, left ventricular diameter shortening rate (FS), left ventricular posterior wall systolic thickness (LVPW,s), and left ventricular posterior wall diastolic thickness (LVPW,d) were decreased, as shown in Fig. 1A. In addition, we also compared the changes of serum CK, CK–MB and LDH between the DOX group and the NS group (Fig. 1B), and evaluate the degree of cardiotoxicity of doxorubicin in rats. In conclusion, It indicated that the rats presented the typical pathological features of myocardial damage.

The damage severity was further verified by H&E staining of Myocardial cell. In Fig. 1C, the rat myocardial cells in the NS group are arranged orderly and the texture structure is clear. On the contrary, the myocardial cells in the DOX group was more significantly edema, some myocardial nuclei were large and stained deeply and there were many vacuoles near the nuclei, the obvious infiltration of inflammatory cells can be seen in the stroma, and the myocardial fibers are dissolved and broken. Consequently, combined with the histopathological manifestatiion results, doxorubicin can affect the normal physiological state of the heart.

## Metabolomics analysis

Plasma samples of rats were analyzed by UPLC–Q–TOF/MS to obtain significantly changed metabolites. The original mass spectra data were analyzed with SIMCA software (version 12.0, Sweden) for multivariate statistical analysis respectively. Then calculated PCA (Fig. 2A, E) and PLS–DA (Fig. 2B, F). The results showed complete separation of the heart between the control group and the doxorubicin injury groups in both negative and positive ionization mode, which were described by high values of R2Y (0.996 and 0.996) and Q2(0.665 and 0.665) parameters. We also performed permutation tests (Fig. 2C, G), and the results showed that the PLS–DA model was not over–fitted and had high reliability. The model validation diagram is used to diagnose, and the number of tests is set to 200. The obtained model validation diagram proves that the PLS–DA model has no over–fitting and high reliability. Meanwhile, S–plot load plot (Fig. 2D, H) showed that the farther metabolites from the central origin on the "S" curve, the greater the VIP value, the greater the contribution. All the differential endogenous metabolites meet the requirements of VIP > 1.5 and $p < 0.05$. By further $MS^2$ identification, 21 significantly changed ions were matched with endogenous metabolites from HMDB database (Table 1), 12 of the identified metabolites were down–regulated and 9 were up–regulated. Next, we will diagnose the 21 differential metabolites diagnostic Significance by two ways: ROC curve and cluster analysis. The ROC curve (Fig. 2J) shows that the area of the 21 metabolites under the curve are all greater than 0.7, the heat map (Fig. 2I) results showed that the content changes of 21 biomarkers in the NS group and the DOX group were significantly different, indicating that they had better accuracy in the diagnosis of heart failure induced by doxorubicin. Based on the KEGG pathway enrichment analysis and topological analysis of MetPA database (Fig. 2K), we can intuitively see that these differential metabolites are participate in a variety of metabolic pathways, among which the metabolic pathways with more influential in heart failure include the

Phenylalanine, tyrosine and tryptophan biosynthesis, the D–glutamine and D–glutamate metabolism, the Phenylalanine metabolism and the Biosynthesis of unsaturated fatty acids, etc. Through these results, we found that HF mainly involves energy metabolism, amino acid metabolism, fatty acid metabolism and glycerophospholipid metabolism disorders.

## Proteomic analysis

Utilization of TMT–based quantitative proteomics, we identified 29,483 peptides in the rats heart tissue samples of the two groups and identified 3,727 protein (Supplementary 2), among which 278 proteins were significantly altered (fold change > 1.2 or < 0.83, $p < 0.05$) as a result of doxorubicin treatments. In details, 118 proteins were up–regulated and 160 proteins were down–regulated in adriamycin treated group (Supplementary 2). In order to better understand which functions or biological pathways are significantly affected by biological processing, we annotated 278 differential proteins by Blast2Go software (https://www.blast2go.com/) for GO function. It can be seen that significant changes have taken place in the top 20 GO terms (Fig. 3A): Biological processes such as the generation of precursor metabolites, ATP metabolic process; Molecular functions such as glutathione binding, antioxidant activity; Cellular components such as mitochondrial envelope, extracellular space, extracellular region. Notably, to understand the metabolic or signaling pathways that these proteins may be involved in, we performed KEGG pathway (Fig. 3B) annotation and found that significant changes have taken place in important pathways such as Glutathione metabolism, Drug metabolism–cytochrome P450, Cardiac muscle contraction, Fructose and mannose metabolism, Glycolysis/Gluconeogenesis, Complement and coagulation. However, the mechanism is still not clear and needs further clarification.

## Integrated proteomics and metabolomics analysis

To associate the proteomics data with the metabolomics data, we conducted a joint pathway analysis with differential metabolites and proteins. We found that 25 differential proteins (Table 2) were closely related to the differential metabolites. The results revealed that several metabolic pathways were significantly targeted, including fatty acid metabolism, glycolysis, amino acid metabolism, glycerol phospholipid metabolism, glutathione metabolism and myocardial contraction (Fig. 4), further relating these pathways to the occurrence of heart failure. In fatty acid metabolism, carnitine substances such as L–Octanoylcarnitine and L–palmitoylcarnitine and proteins such as acetyl–CoAacyltransferase2 and acyl–CoA dehydrogenase, C–2toC–3shortchain affect the decrease of the fatty acid beta–oxidation catalytic enzyme, suggesting that the energy supply process of fatty acid β–oxidation in cardiomyocytes is affected. The up–regulation of protein phosphatase and the reduction of glycolytic enzymes in glycolysis indicate that the glycolysis process of cardiomyocytes is also affected. Meanwhile, the decrease of alpha–Ketoglutarate, ATP synthase, H+ transporting, mitochondrial Fo complex, subunit F6 and succinate–CoA ligase ADP–forming beta subunit in TCA cycle indicated that the efficiency of TCA cycle was reduced. The decrease of superoxide dismutase 2, mitochondrial (SOD), cytochrome c (Cyt C), adenylate kinase 4 (AK4) and FK506 binding protein 4 (FKB4) suggest the level of oxidative stress was higher. Creatine, transthyretin (Ttr), ryanodine receptor 2 (Ryr2) decreased indicates that myocardial

contraction is affected. The decrease of lysophosphatidylcholine (LPCs) and the increase of alpha–linolenic acid suggested that glycerol phospholipid metabolism has been affected. Elevated expression of glutathione–S–transferase represents the imbalance of glutathione metabolism in cardiomyocytes. We speculate that doxorubicin may lead to inadequate myocardial energy supply and accumulation of cardiac reactive oxygen species (ROS) through abnormal fatty acid metabolism and glucose metabolism, which together lead to calcium homeostasis affecting cardiac contractile function and leads to heart failure ultimately.

However, we found that most of these proteins were downstream effector proteins through KEGG analysis, so it is particularly important to find the upstream key target proteins. Then we use the protein prediction function of the STRING database to select the proteins that play an important role in proteomics results to predict the upstream proteins based on the known doxorubicin target proteins, and we enrich the key target protein tyrosine–protein phosphatase non–receptor type 1 (PTP1B). Through the KEGG database, we can find that PTP1B can inhibit insulin receptor substrate (IRS), PI3K achieves GLUT4 transport by activating Akt/PKB and PKC cascade, and protein synthesis by mTOR and downstream components after protein kinase B (Akt) activation. PP2A has an inhibitory effect on Akt and PKC ζ. The negative feedback signal from Akt/PKB, PKC ζ and p70S6K leads to serine phosphorylation and inactivation of IRS signal transduction, resulting in the formation of HIF–α, and there is a certain correlation between HK2 and HIF–α, which further affects glycolysis. When oxidative stress occurs, protein kinase C (protein kinase C, PKC) and phosphatidylinositol 3 kinase (PI3K) promotes the dissociation of Nrf2 and Keap1. Nrf2 enters the nucleus and binds to antioxidant response elements (AREs) to generate GSTs and SOD, thus exerting the role of antioxidant damage. With the degradation of Nrf2, the activation is terminated. AK4 and FKBP4 also affect oxidative stress, produce Ttr and Ryr2 to release $Ca2^{+}$, stimulate CytC generation, at the same time block the scavenging of ROS free radicals and lead to apoptosis. In Fig. 5, it can be seen PTP1B is in the upstream position of the pathway, so we speculate that it is one of the key targets upstream.

### Protein expression in cardiac tissue of two groups

Previous studies have shown that PTP1B may be a key upstream target in HF. In order to test our conjecture, we detected the expression of IRS, HIF–1α, Nrf2 and HK–2 in the downstream nodes of PTP1B. Results as shown in Fig. 6, we found that compared with the NS group, the expression level of IRS protein increased significantly, while the expression levels of P–IRS1, HIF–1α, Nrf2 and HK–2 protein decreased significantly in the DOX group. It is suggested that the upregulation of PTP1B protein will inhibit IRS phosphorylation, resulting in decreased P–IRS1 expression, a decrease in the expression of HIF–1α, and inhibition of downstream glycolysis, at the same time, it can also cause decreased expression of Nrf2, leading to increased levels of oxidative stress in the body. Promote the occurrence of HF through energy metabolism and oxidative stress.

# Discussion

Studies have shown that protein PTP1B, a molecular target for anti–type II diabetes, obesity and cancer treatment, can regulate the level of protein tyrosine phosphorylation in cells(Chen et al., 2018). PTP1B is widely expressed in cardiovascular tissues, especially in the heart and endothelial cells, so we believe that PTP1B is an interesting molecular target for the treatment of cardiovascular and metabolic diseases(Thiebaut et al., 2016). However, is not very clear about the mechanism of PTP1B with the HF. In our research, we found that target protein PTP1B can cause damage to the heart through energy metabolism, oxidative stress and calcium homeostasis disorders.

## Energy metabolism

The heart is the most energy-consuming organ of the body and requires a large amount of ATP to provide energy. Removing mitochondrial oxidative phosphorylation, the main source of ATP is fatty acid oxidation, followed by glucose oxidation, amino acid oxidation and so on. In heart failure, energy production is converted from fatty acid beta-oxidation to glucose oxidation, which contributes to the progressive deterioration of cardiac function in hypertrophy and heart failure(Dong et al., 2017).In this study, carnitine and Acaa2, Acads showed a downward trend, which proved that the oxidation ability of fatty acids was affected and cardiac function was impaired(Bertero and Maack, 2018). Studies in knockdown PTP1B mice have shown that PTP1B protein has significant effects on insulin sensitivity, glucose homeostasis and lipid metabolism(Owen et al., 2013; Zhang et al., 2016). PTP1B attenuates insulin signal transduction by removing tyrosine from activated insulin receptors and IRS-1, triggers PI3K activation and catalyzes the lipid product phosphatidylinositol (3,4,5)-triphosphate (PIP3), which in turn leads to the activation of protein kinase B (Akt) to stimulate GLUT4 translocation affecting glucose absorption(Nguyen et al., 2018; Ormazabal et al., 2018; Riehle and Abel, 2016). Meanwhile, PTP1B activates mTOR through the Akt/PI3K pathway, thereby affecting HIF-1α and HK2, and converts to aerobic glycolysis metabolism(Cheng et al., 2014; Wolf et al., 2011).

Pyruvate can be oxidized by acetyl coenzyme A (acetyl-CoA) or as a complementary substrate to supplement the intermediate products of the TCA cycle(Turer et al., 2019). Therefore, when the rate-limiting enzyme HK-2, which reacts with glycolytic capacity, and phosphofructokinase (Pfkp, Pfkm), which is a key regulator in glycolysis decrease, leading to a decrease in glucose utilization, pyruvate also decreases(Gibb et al., 2017; Jiao et al., 2018). Meanwhile, the level of non-essential amino acid glutamine also plays a role in regulating cellular energy homeostasis, which is converted into a-ketoglutarate, an intermediate of the citric acid cycle, by a two-step process(Tebay et al., 2015). The decrease of metabolite α-ketoglutaric acid, differential protein atp5j and sucla2 indicated the decrease of TCA cycle efficiency. This reflects the reduced TCA cycle efficiency of cardiomyocytes and the inability to provide sufficient ATP, indicating that fatty acid oxidation and glycolysis can affect the downstream TCA cycle, resulting in a decrease in ATP.

In the study, we found that the lysophosphatidylcholine LPCs decreased significantly, which has been demonstrated to be accompanied by a decrease in ejection fraction (EF) when heart failure occurs, and a decrease in EF is associated with disorders in phospholipid metabolism(Marcinkiewicz-Siemion et al.,

2018). Combined with the above factors, PTP1B protein affected the phosphorylation of insulin receptor substrate protein IRS, caused disorders of glycolysis and lipid metabolism, and accompanied by the imbalance of glutamine regulatory capacity homeostasis, which together led to the impact of TCA cycle, resulting in the reduction of cardiac energy supply, and then the occurrence of heart failure.

### Oxidative stress

Oxidative stress is an important feature of the onset and development of many diseases (including cardiovascular diseases), and one of the common features that play an important role in the pathophysiology of heart failure is chronic oxidative stress(Belch et al., 1991; Hill and Singal, 1997; Zima et al., 2016). Gamma 1-glutamyl -1- cysteine glycine(GSH), a tripeptide that can prevent oxidative stress and can be oxidized to form glutathione two sulfur (GSSG)，when the ratio between oxidized and reduced GSH increases and glutathione mixed with disulfide, it will play a pathogenic factor in cardiovascular diseases(Chevallier et al., 2020; Lu, 2013; Zima et al., 2016).PTP1B increases glutathione S-transferase (GSTs) protein levels by stimulating insulin receptor substrates, activating downstream PI3K, Akt/protein kinase B, ribosomal p70S6 kinase (p70S6K), and PKC(Kim et al., 2006). The increased expression of glutathione-S-transferase represents the imbalance of glutathione metabolism in cardiomyocytes, depletion of GSH increases and the ratio of GSH/GSSG decreases, which enhanced oxidative stress from reactive oxygen species (ROS) in cardiomyocytes(Cramer et al., 2017; Ma et al., 2018).

On the other hand, Nrf2 is widely recognized as a transcription factor activated by oxidative stress, and cells lacking Nrf2 can lead to mitochondrial dysfunction, resulting in increased ROS and impaired antioxidant capacity(Tebay et al., 2015).Besides, studies have shown that Ryr2 can activate the synthesis of GSH(Wei et al., 2020). At the same time, the decrease of differential protein superoxide dismutase 2 (SOD2) and CytC is also considered as an indicator of the elevated level of oxidative stress in the body(Sun Jang et al., 2009). Interestingly, Ryr2 plays a contradictory role in cancer, where Ryr2 is usually up-regulated to promote the development of cancer by inhibiting apoptosis and increasing cell proliferation or activating AKR and NQO1 enzymes of some carcinogens(Tebay et al., 2015).

### Calcium homeostasis

Calcium homeostasis is a central point in maintaining normal cardiac contractility in heart failure. Dysfunction of systolic Ca transport caused by dysfunction of the 2 type ryanodine receptor (RyR2) in the sarcoplasmic reticulum is associated with a variety of heart diseases, including catecholaminergic polymorphic ventricular tachycardia (CPVT), atrial fibrillation (AF) and HF(Connell et al., 2020).In cardiomyocytes, Ca2+ enters through L-type Ca2+ channels, which mediate the opening of RyR2 channels, allowing Ca2+ to contract from sarcoplasmic reticulum (SR) to cytoplasm, thus releasing energy from ATP hydrolysis by binding to enzymes on mitochondria(Gonano and Vila Petroff, 2020; Kaplan et al., 2003). When RyR2 deficiency or expression decreases, Ca2+ spontaneously leaks from the sarcoplasmic reticulum(Suetomi et al., 2011), which influences the calcium homeostasis of cardiomyocytes, reduces the production of ATP from mitochondria, and lead to heart failure due to cardiac systolic dysfunction. Also, ATP derived from the conversion of phosphokinase (CK) to creatine is

an important chemical source of myocardial contraction, and the down-regulation of creatine also indicates that cardiac systolic and diastolic function is affected during heart failure(Haris et al., 2014). This study demonstrates that oxidative stress leads to the expression of Ttr protein(Zhang et al., 2018), which subsequently affects the low expression of RyR2, leading to Ca2+ homeostasis disorders affecting myocardial contraction.

# Abbreviations

**UPLC-Q-TOF/MS**: Ultra-high performance liquid chromatography tandem quadrupole time-of-flight mass spectrometry, **HF**: Heart failure, **TMT**: Tandem mass tag, **EF**: Ejection fraction, **LDH**: Lactate dehydrogenase, **CK**:Troponin kinase, CK–MB: creatine kinase isoenzymes, **H&E**: Hematoxylin and eosin, **PCA**: Principal component analysis, **PLS–DA**: Partial least squares–discriminant analysis, **ROC**: Receiver operating characteristic curve, **VIP**: Variable importance in the projection, **LVID,d**: left ventricular volume, **LVID,s**: Systolic left ventricular volume, **FS**: Left ventricular diameter shortening rate, **LVPW,s**: Left ventricular posterior wall systolic thickness, **LVPW,d**: left ventricular posterior wall diastolic thickness, **ROS**: Reactive oxygen species, **PTP1B**: ProteinTyrosine Phosphatase-1B, **IRS**: Insulin receptor substrate, **Ryr2**: Ryanodine receptor 2, **HIF-1α**: Hypoxia inducible factor-1, **HK2**: hexokinase 2.

# Declarations

**Authors'contributions:** YMW and YBL planned and supervised the experiments. SMF, WH, YY, YMW, and LXS analyzed and interpretated the data. Data collection. YY and YMW writing the article. All authors agreed to the publication. The author(s)read and approved the final manuscript.

**Declaration of competing interest:** The authors declare that they have no known competing financial interests or personal relationships that could have appeared to influence the work reported in this paper.

**Funding information:** This work was supported by Tianjin Development Program for Innovation and Entrepreneurship and National Natural Science Foundation of China (No. 81903938).

**Acknowledgement:** We are grateful to the members of the Shanghai Applied Protein Technology Co., Ltd (Shanghai, China) for tandem mass spectrometry (TMT) quantitative proteomics analysis and data interpretation.

# References

Bangalore, S., Maron, D., O'Brien, S., Fleg, J., Kretov, E., Briguori, C., Kaul, U., Reynolds, H., Mazurek, T., Sidhu, M., Berger, J., Mathew, R., Bockeria, O., Broderick, S., Pracon, R., Herzog, C., Huang, Z., Stone, G., Boden, W., Newman, J., Ali, Z., Mark, D., Spertus, J., Alexander, K., Chaitman, B., Chertow, G., Hochman, J. and , J.T.N.E.j.o.m., 2020. Management of Coronary Disease in Patients with Advanced Kidney Disease. 382, 1608-1618.

Belch, J., Bridges, A., Scott, N. and Chopra, M.J.B.h.j., 1991. Oxygen free radicals and congestive heart failure. 65, 245-8.

Bertero, E. and Maack, C.J.N.r.C., 2018. Metabolic remodelling in heart failure. 15, 457-470.

Chen, S., Zhang, Y., Lighthouse, J., Mickelsen, D., Wu, J., Yao, P., Small, E. and Yan, C.J.C., 2020a. A Novel Role of Cyclic Nucleotide Phosphodiesterase 10A in Pathological Cardiac Remodeling and Dysfunction. 141, 217-233.

Chen, T., Wu, D., Chen, H., Yan, W., Yang, D., Chen, G., Ma, K., Xu, D., Yu, H., Wang, H., Wang, T., Guo, W., Chen, J., Ding, C., Zhang, X., Huang, J., Han, M., Li, S., Luo, X., Zhao, J. and Ning, Q.J.B., 2020b. Clinical characteristics of 113 deceased patients with coronavirus disease 2019: retrospective study. 368, m1091.

Chen, X., Gan, Q., Feng, C., Liu, X., Zhang, Q.J.J.o.c.i. and modeling, 2018. Virtual Screening of Novel and Selective Inhibitors of Protein Tyrosine Phosphatase 1B over T-Cell Protein Tyrosine Phosphatase Using a Bidentate Inhibition Strategy. 58, 837-847.

Cheng, S., Quintin, J., Cramer, R., Shepardson, K., Saeed, S., Kumar, V., Giamarellos-Bourboulis, E., Martens, J., Rao, N., Aghajanirefah, A., Manjeri, G., Li, Y., Ifrim, D., Arts, R., van der Veer, B., van der Meer, B., Deen, P., Logie, C., O'Neill, L., Willems, P., van de Veerdonk, F., van der Meer, J., Ng, A., Joosten, L., Wijmenga, C., Stunnenberg, H., Xavier, R. and Netea, M.J.S., 2014. mTOR- and HIF-1α-mediated aerobic glycolysis as metabolic basis for trained immunity. 345, 1250684.

Chevallier, V., Andersen, M., Malphettes, L.J.B. and bioengineering, 2020. Oxidative stress-alleviating strategies to improve recombinant protein production in CHO cells. 117, 1172-1186.

Chirinos, J., Zhao, L., Jia, Y., Frej, C., Adamo, L., Mann, D., Shewale, S., Millar, J., Rader, D., French, B., Brandimarto, J., Margulies, K., Parks, J., Wang, Z., Seiffert, D., Fang, J., Sweitzer, N., Chistoffersen, C., Dahlbäck, B., Car, B., Gordon, D., Cappola, T. and Javaheri, A.J.C., 2020. Reduced Apolipoprotein M and Adverse Outcomes Across the Spectrum of Human Heart Failure. 141, 1463-1476.

Cifani, P. and Kentsis, A.J.P., 2017. Towards comprehensive and quantitative proteomics for diagnosis and therapy of human disease. 17.

Connell, P., Word, T. and Wehrens, X.J.E.o.o.t.t., 2020. Targeting pathological leak of ryanodine receptors: preclinical progress and the potential impact on treatments for cardiac arrhythmias and heart failure. 24, 25-36.

Cramer, S., Saha, A., Liu, J., Tadi, S., Tiziani, S., Yan, W., Triplett, K., Lamb, C., Alters, S., Rowlinson, S., Zhang, Y., Keating, M., Huang, P., DiGiovanni, J., Georgiou, G. and Stone, E.J.N.m., 2017. Systemic depletion of L-cyst(e)ine with cyst(e)inase increases reactive oxygen species and suppresses tumor growth. 23, 120-127.

Dong, Z., Zhao, P., Xu, M., Zhang, C., Guo, W., Chen, H., Tian, J., Wei, H., Lu, R. and Cao, T.J.S.r., 2017. Astragaloside IV alleviates heart failure via activating PPARα to switch glycolysis to fatty acid β-oxidation. 7, 2691.

Eisenberg, E., Di Palo, K. and Piña, I.J.C.c., 2018. Sex differences in heart failure. 41, 211-216.

Fu, H., Sanada, S., Matsuzaki, T., Liao, Y., Okuda, K., Yamato, M., Tsuchida, S., Araki, R., Asano, Y., Asanuma, H., Asakura, M., French, B., Sakata, Y., Kitakaze, M. and Minamino, T.J.C.r., 2016. Chemical Endoplasmic Reticulum Chaperone Alleviates Doxorubicin-Induced Cardiac Dysfunction. 118, 798-809.

Gibb, A., Lorkiewicz, P., Zheng, Y., Zhang, X., Bhatnagar, A., Jones, S. and Hill, B.J.T.B.j., 2017. Integration of flux measurements to resolve changes in anabolic and catabolic metabolism in cardiac myocytes. 474, 2785-2801.

Gonano, L. and Vila Petroff, M.J.C.r., 2020. Direct Modulation of RyR2 Leading to a TRICky Ca Balance: The Effects of TRIC-A on Cardiac Muscle. 126, 436-438.

Haris, M., Singh, A., Cai, K., Kogan, F., McGarvey, J., Debrosse, C., Zsido, G., Witschey, W., Koomalsingh, K., Pilla, J., Chirinos, J., Ferrari, V., Gorman, J., Hariharan, H., Gorman, R. and Reddy, R.J.N.m., 2014. A technique for in vivo mapping of myocardial creatine kinase metabolism. 20, 209-14.

Hill, M. and Singal, P.J.C., 1997. Right and left myocardial antioxidant responses during heart failure subsequent to myocardial infarction. 96, 2414-20.

Hoffman, J., Lyu, Y., Pletcher, S. and Promislow, D.J.E.i.b., 2017. Proteomics and metabolomics in ageing research: from biomarkers to systems biology. 61, 379-388.

Jiao, L., Zhang, H., Li, D., Yang, K., Tang, J., Li, X., Ji, J., Yu, Y., Wu, R., Ravichandran, S., Liu, J., Feng, G., Chen, M., Zeng, Y., Deng, R. and Zhu, X.J.A., 2018. Regulation of glycolytic metabolism by autophagy in liver cancer involves selective autophagic degradation of HK2 (hexokinase 2). 14, 671-684.

Kaplan, P., Babusikova, E., Lehotsky, J., Dobrota, D.J.M. and biochemistry, c., 2003. Free radical-induced protein modification and inhibition of Ca2+-ATPase of cardiac sarcoplasmic reticulum. 248, 41-7.

Kim, S., Abdelmegeed, M., Novak, R.J.T.J.o.p. and therapeutics, e., 2006. Identification of the insulin signaling cascade in the regulation of alpha-class glutathione S-transferase expression in primary cultured rat hepatocytes. 316, 1255-61.

Lu, S.J.B.e.b.a., 2013. Glutathione synthesis. 1830, 3143-53.

Ma, R., Ji, T., Zhang, H., Dong, W., Chen, X., Xu, P., Chen, D., Liang, X., Yin, X., Liu, Y., Ma, J., Tang, K., Zhang, Y., Peng, Y., Lu, J., Zhang, Y., Qin, X., Cao, X., Wan, Y. and Huang, B.J.N.c.b., 2018. A Pck1-directed glycogen metabolic program regulates formation and maintenance of memory CD8 T cells. 20, 21-27.

Marcinkiewicz-Siemion, M., Ciborowski, M., Ptaszynska-Kopczynska, K., Szpakowicz, A., Lisowska, A., Jasiewicz, M., Waszkiewicz, E., Kretowski, A., Musial, W., Kaminski, K.J.J.o.p. and analysis, b., 2018. LC-MS-based serum fingerprinting reveals significant dysregulation of phospholipids in chronic heart failure. 154, 354-363.

Marwick, T.J.J.o.n.m.o.p., Society of Nuclear Medicine, 2015. The role of echocardiography in heart failure. 31S-38S.

Mato, J., Martínez-Chantar, M. and Lu, S.J.H., 2014. Systems biology for hepatologists. 60, 736-43.

Maurer, M. and Packer, M.J.J.C.i., 2020. How Should Physicians Assess Myocardial Contraction?: Redefining Heart Failure With a Preserved Ejection Fraction. 13, 873-878.

Nguyen, T., Schwarzer, M., Schrepper, A., Amorim, P., Blum, D., Hain, C., Faerber, G., Haendeler, J., Altschmied, J. and Doenst, T.J.J.o.t.A.H.A., 2018. Increased Protein Tyrosine Phosphatase 1B (PTP1B) Activity and Cardiac Insulin Resistance Precede Mitochondrial and Contractile Dysfunction in Pressure-Overloaded Hearts. 7.

Ormazabal, P., Scazzocchio, B., Varì, R., Santangelo, C., D'Archivio, M., Silecchia, G., Iacovelli, A., Giovannini, C. and Masella, R.J.I.j.o.o., 2018. Effect of protocatechuic acid on insulin responsiveness and inflammation in visceral adipose tissue from obese individuals: possible role for PTP1B. 42, 2012-2021.

Owen, C., Lees, E., Grant, L., Zimmer, D., Mody, N., Bence, K. and Delibegović, M.J.D., 2013. Inducible liver-specific knockdown of protein tyrosine phosphatase 1B improves glucose and lipid homeostasis in adult mice. 56, 2286-96.

Rayner, J., Peterzan, M., Watson, W., Clarke, W., Neubauer, S., Rodgers, C. and Rider, O.J.C., 2020. Myocardial Energetics in Obesity: Enhanced ATP Delivery Through Creatine Kinase With Blunted Stress Response. 141, 1152-1163.

Riehle, C. and Abel, E.J.C.r., 2016. Insulin Signaling and Heart Failure. 118, 1151-69.

Rinschen, M., Ivanisevic, J., Giera, M. and Siuzdak, G.J.N.r.M.c.b., 2019. Identification of bioactive metabolites using activity metabolomics. 20, 353-367.

Sliwa, K.J.E.h.j., 2020. Heart failure can affect everyone: the ESC Geoffrey Rose lecture. 41, 1298-1306.

Sueki, A., Stein, F., Savitski, M., Selkrig, J. and Typas, A.J.m., 2020. Systematic Localization of Escherichia coli Membrane Proteins. 5.

Suetomi, T., Yano, M., Uchinoumi, H., Fukuda, M., Hino, A., Ono, M., Xu, X., Tateishi, H., Okuda, S., Doi, M., Kobayashi, S., Ikeda, Y., Yamamoto, T., Ikemoto, N. and Matsuzaki, M.J.C., 2011. Mutation-linked defective interdomain interactions within ryanodine receptor cause aberrant Ca²⁺ release leading to catecholaminergic polymorphic ventricular tachycardia. 124, 682-94.

Sun Jang, J., Piao, S., Cha, Y., Kim, C.J.J.o.c.b. and nutrition, 2009. Taurine Chloramine Activates Nrf2, Increases HO-1 Expression and Protects Cells from Death Caused by Hydrogen Peroxide. 45, 37-43.

Tang, X., Pan, L., Zhao, S., Dai, F., Chao, M., Jiang, H., Li, X., Lin, Z., Huang, Z., Meng, G., Wang, C., Chen, C., Liu, J., Wang, X., Ferro, A., Wang, H., Chen, H., Gao, Y., Lu, Q., Xie, L., Han, Y. and Ji, Y.J.C., 2020. SNO-MLP (S-Nitrosylation of Muscle LIM Protein) Facilitates Myocardial Hypertrophy Through TLR3 (Toll-Like Receptor 3)-Mediated RIP3 (Receptor-Interacting Protein Kinase 3) and NLRP3 (NOD-Like Receptor Pyrin Domain Containing 3) Inflammasome Activation. 141, 984-1000.

Tebay, L., Robertson, H., Durant, S., Vitale, S., Penning, T., Dinkova-Kostova, A., Hayes, J.J.F.r.b. and medicine, 2015. Mechanisms of activation of the transcription factor Nrf2 by redox stressors, nutrient cues, and energy status and the pathways through which it attenuates degenerative disease. 88, 108-146.

Thiebaut, P., Besnier, M., Gomez, E., Richard, V.J.J.o.m. and cardiology, c., 2016. Role of protein tyrosine phosphatase 1B in cardiovascular diseases. 101, 50-57.

Turer, A., Altamirano, F., Schiattarella, G., May, H., Gillette, T., Malloy, C., Merritt, M.J.J.o.m. and cardiology, c., 2019. Remodeling of substrate consumption in the murine sTAC model of heart failure. 134, 144-153.

Wei, Y., Lu, M., Mei, M., Wang, H., Han, Z., Chen, M., Yao, H., Song, N., Ding, X., Ding, J., Xiao, M. and Hu, G.J.N.c., 2020. Pyridoxine induces glutathione synthesis via PKM2-mediated Nrf2 transactivation and confers neuroprotection. 11, 941.

Wolf, A., Agnihotri, S., Micallef, J., Mukherjee, J., Sabha, N., Cairns, R., Hawkins, C. and Guha, A.J.T.J.o.e.m., 2011. Hexokinase 2 is a key mediator of aerobic glycolysis and promotes tumor growth in human glioblastoma multiforme. 208, 313-26.

Zhang, P., Guan, X., Yang, M., Zeng, L. and Liu, C.J.T.S.o.t.t.e., 2018. Roles and potential mechanisms of selenium in countering thyrotoxicity of DEHP. 732-739.

Zhang, X., Tian, J., Li, J., Huang, L., Wu, S., Liang, W., Zhong, L., Ye, J. and Ye, F.J.B.j.o.p., 2016. A novel protein tyrosine phosphatase 1B inhibitor with therapeutic potential for insulin resistance. 173, 1939-49.

Zima, A., Mazurek, S.J.R.o.p., biochemistry and pharmacology, 2016. Functional Impact of Ryanodine Receptor Oxidation on Intracellular Calcium Regulation in the Heart. 171, 39-62.

# Tables

Table 1. Potential biomarkers were selected in plasma of COX-treated rats and normal rats.

| No. | $T_R$ (min) | Compound | Molecular Formula | m/z Obsd | m/z Calcd | Error (ppm) | Ion mode | Treatment group VS Control group |
|---|---|---|---|---|---|---|---|---|
| 1 | 0.93 | Tryptophan | $C_{11}H_{12}N_2O_2$ | 227.0796 | 227.0796 | 0 | + | ↓** |
| 2 | 0.92 | Tyrosine | $C_9H_{11}NO_3$ | 182.0817 | 182.0819 | 1.10 | + | ↓* |
| 3 | 0.80 | Glutamine | $C_5H_{10}N_2O_3$ | 169.0589 | 169.0587 | –1.18 | + | ↓* |
| 4 | 0.83 | Pyroglutamine | $C_5H_8N_2O_2$ | 129.0664 | 129.0665 | 0.77 | + | ↓* |
| 5 | 11.31 | Alpha–Ketoglutarate | $C_5H_6O_5$ | 184.9852 | 184.9864 | 6.49 | + | ↓** |
| 6 | 4.41 | Sphingosine | $C_{18}H_{37}NO_2$ | 300.2903 | 300.2902 | –0.33 | + | ↑* |
| 7 | 2.80 | L–Octanoylcarnitine | $C_{15}H_{29}NO_4$ | 288.2175 | 288.2169 | –2.08 | + | ↓* |
| 8 | 0.93 | Phenylpyruvic acid | $C_9H_8O_3$ | 165.0552 | 165.0547 | –3.03 | + | ↑* |
| 9 | 2.45 | Prolylhydroxyproline | $C_{10}H_{16}N_2O_4$ | 251.1008 | 251.1014 | 2.39 | + | ↓* |
| 10 | 5.37 | LysoPC(20:4(8Z,11Z,14Z,17Z)/0:0) | $C_{28}H_{50}NO_7P$ | 566.3223 | 566.3218 | –0.80 | + | ↓** |
| 11 | 6.25 | LysoPC(18:1(11Z)/0:0) | $C_{26}H_{52}NO_7P$ | 544.3379 | 544.3381 | 0.37 | + | ↑* |
| 12 | 5.48 | L–palmitoyl carnitine | $C_{23}H_{45}NO_4$ | 400.3427 | 400.3432 | 1.25 | + | ↓** |
| 13 | 5.66 | Alpha–Linolenic acid | $C_{18}H_{30}O_2$ | 279.2324 | 279.2314 | –3.58 | + | ↑* |
| 14 | 6.03 | Tetradecanedioic acid | $C_{14}H_{26}O_4$ | 297.1468 | 297.15 | 10.77 | + | ↑* |
| 15 | 6.28 | Trimethoprim | $C_{14}H_{18}N_4O_3$ | 291.1457 | 291.1437 | –6.87 | + | ↑** |
| 16 | 5.94 | Cortolone–3–glucuronide | $C_{27}H_{42}O_{11}$ | 565.2625 | 565.2661 | 6.37 | + | ↓** |
| 17 | 2.53 | Creatine | C4H9N3O2 | 130.0617 | 130.0623 | 4.61 | – | ↓* |
| 18 | 5.28 | LysoPE(0:0/24:6(6Z,9Z,12Z,15Z,18Z,21Z)) | $C_{29}H_{48}NO_7P$ | 552.3090 | 552.3085 | –0.91 | – | ↑* |
| 19 | 7.69 | Eicosapentaenoic Acid | $C_{20}H_{30}O_2$ | 301.2168 | 301.2188 | 6.64 | – | ↓* |
| 20 | 5.93 | 12,13–epoxy–9,15–octadecadienoic acid | $C_{18}H_{30}O_3$ | 293.2117 | 293.2119 | 0.68 | – | ↑* |
| 21 | 5.83 | 11,14,17–Eicosatrienoic acid | $C_{20}H_{34}O_2$ | 305.2481 | 305.2500 | 6.22 | – | ↑** |

The change trend is compared between the DOX group and the NS group. ↑ and ↓ represent up- and down-regulation. *$p$□0.05. **$p$□0.01.

Table 2. Differentially regulated proteins selected by integration analysis.

| No. | Protein description | Gene Name | LP/NS Ratio | Regulated Type |
|---|---|---|---|---|
| 1 | glutathione S–transferase alpha 1 | Gsta1 | 1.31 | ↑* |
| 2 | microsomal glutathione S–transferase 1 | Mgst1 | 1.27 | ↑** |
| 3 | glutathione S–transferase pi 1 | Gstp1 | 1.19 | ↑** |
| 4 | glutathione S–transferase mu 2 | Gstm2 | 1.17 | ↑* |
| 5 | glutathione S–transferase mu 1 | Gstm1 | 1.13 | ↑** |
| 6 | glutathione S–transferase alpha 4 | Gsta4 | 1.10 | ↑* |
| 7 | enolase 3 | Eno3 | 0.85 | ↓* |
| 8 | phosphoglycerate mutase 2 | Pgam2 | 0.87 | ↓* |
| 9 | hexokinase 2 | Hk2 | 0.84 | ↓** |
| 10 | phosphofructokinase, muscle | Pfkm | 0.91 | ↓* |
| 11 | transthyretin | Ttr | 0.61 | ↓* |
| 12 | ryanodine receptor 2 | Ryr2 | 0.87 | ↓** |
| 13 | acetyl–CoA acyltransferase 2 | Acaa2 | 0.83 | ↓** |
| 14 | acyl–CoA dehydrogenase, C–2 to C–3 short chain | Acads | 0.86 | ↓** |
| 15 | ATP synthase, H+ transporting, mitochondrial Fo complex, subunit F6 | Atp5pf | 0.91 | ↓* |
| 16 | succinate–CoA ligase ADP–forming beta subunit | Sucla2 | 0.90 | ↓* |
| 17 | superoxide dismutase 2, mitochondrial | Sod2 | 0.84 | ↓* |
| 18 | cytochrome c | Cyt C | 0.86 | ↓* |
| 19 | adenylate kinase 4 | AK4 | 0.91 | ↓** |
| 20 | FK506 binding protein 4 | Fkbp4 | 0.88 | ↓* |
| 21 | COX14, cytochrome c oxidase assembly factor | Cox14 | 0.85 | ↓* |
| 22 | cytochrome c oxidase subunit 5B | Cox5b | 0.90 | ↓* |
| 23 | cytochrome c oxidase subunit 5A | Cox5a | 0.90 | ↓** |
| 24 | cytochrome c oxidase subunit 7A1 | Cox7a1 | 0.85 | ↓* |
| 25 | protein phosphatase 2 | PP2A | 1.10 | ↑* |

↑ and ↓ represent up- and down-regulation, *$p$<0.05, *$p$< 0.01.

# Figures

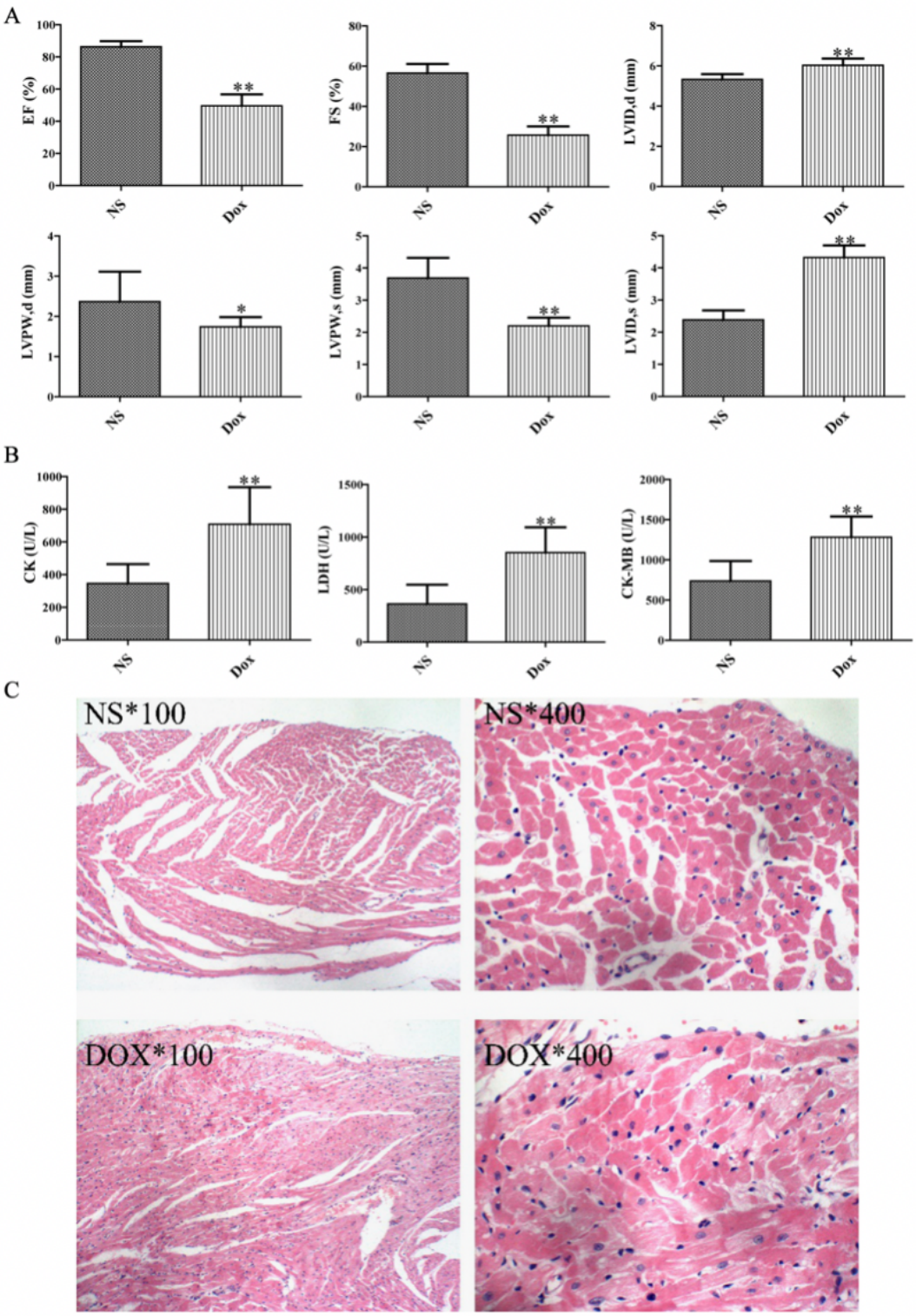


## Figure 1

Effects of doxorubicin-induced heart pathology and biochemistry changes in heart failure. (A) Echocardiographic evaluation of rat hearts. (B) Biochemical indices in rat serum. (C)Staining results of rat cardiomyocytes. (*p < 0.05, **p < 0.01. *,100: magnification 100 x; *,400: magnification 400 x).

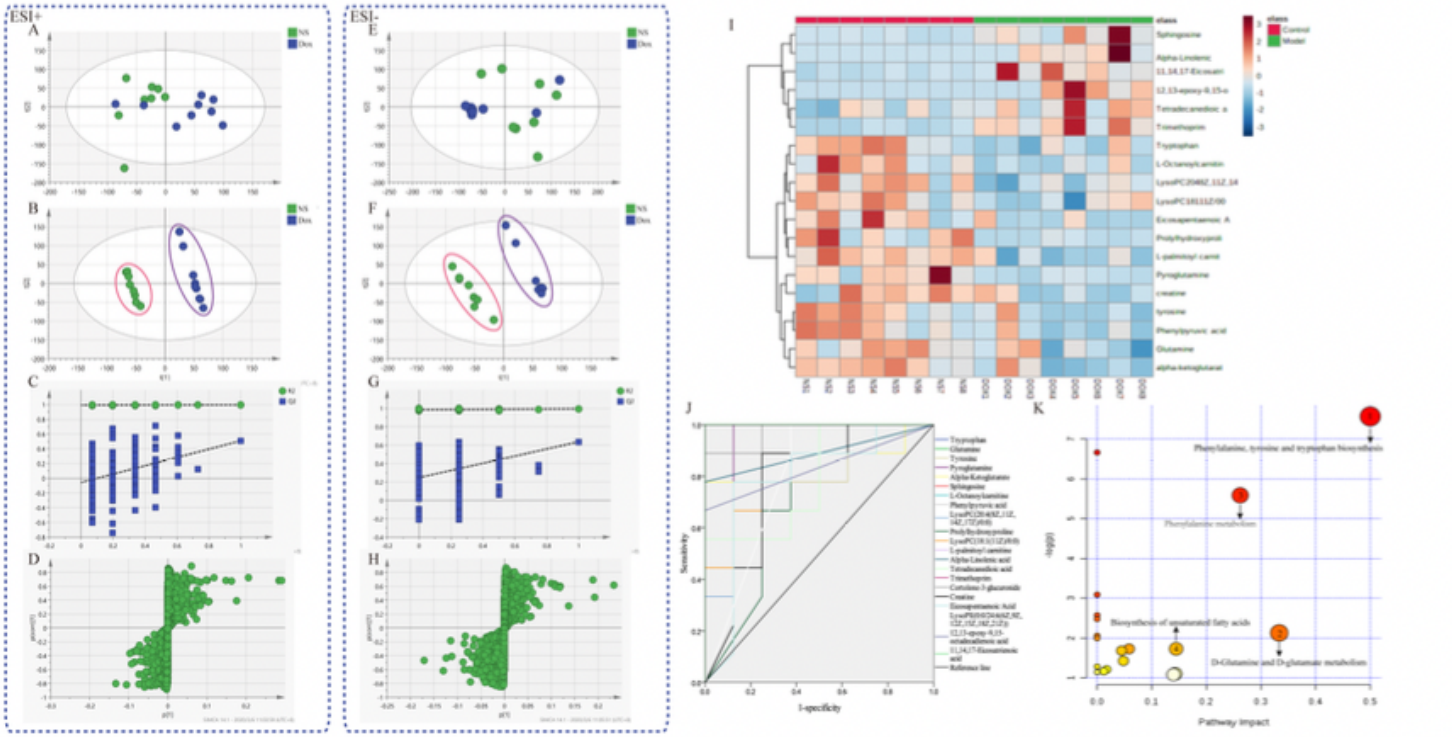

## Figure 2

The metabolic profiles and metabolite analysis of plasma samples. (A) PCA score plots (ESI+) for comprehensive metabonomic data of plasma samples. Models include the control and COX–treated rat (3mg/kg). (B) PLS–DA models (ESI+) of UPLC–Q–TOF/MS metabonomics data for control group and Models include the control and COX–treated rat (3mg/kg) (C) Model validation diagram in positive ion mode. (D) S–plot load diagram in positive ion mode. (E) PCA score plots (ESI–) for comprehensive metabonomic data of plasma samples. Models include the control and COX–treated rat (3mg/kg). (F) PLS–DA models (ESI–) of UPLC–Q–TOF/MS metabonomics data for control group and Models include the control and COX–treated rat (3mg/kg). (G) Model validation diagram in negative ion mode. (H) S–plot load diagram in negative ion mode. (I) Heat map for metabolites. (J) Diagnostic significance of ROC curve analysis for metabolites. (K) Metabolic pathway map analysis.

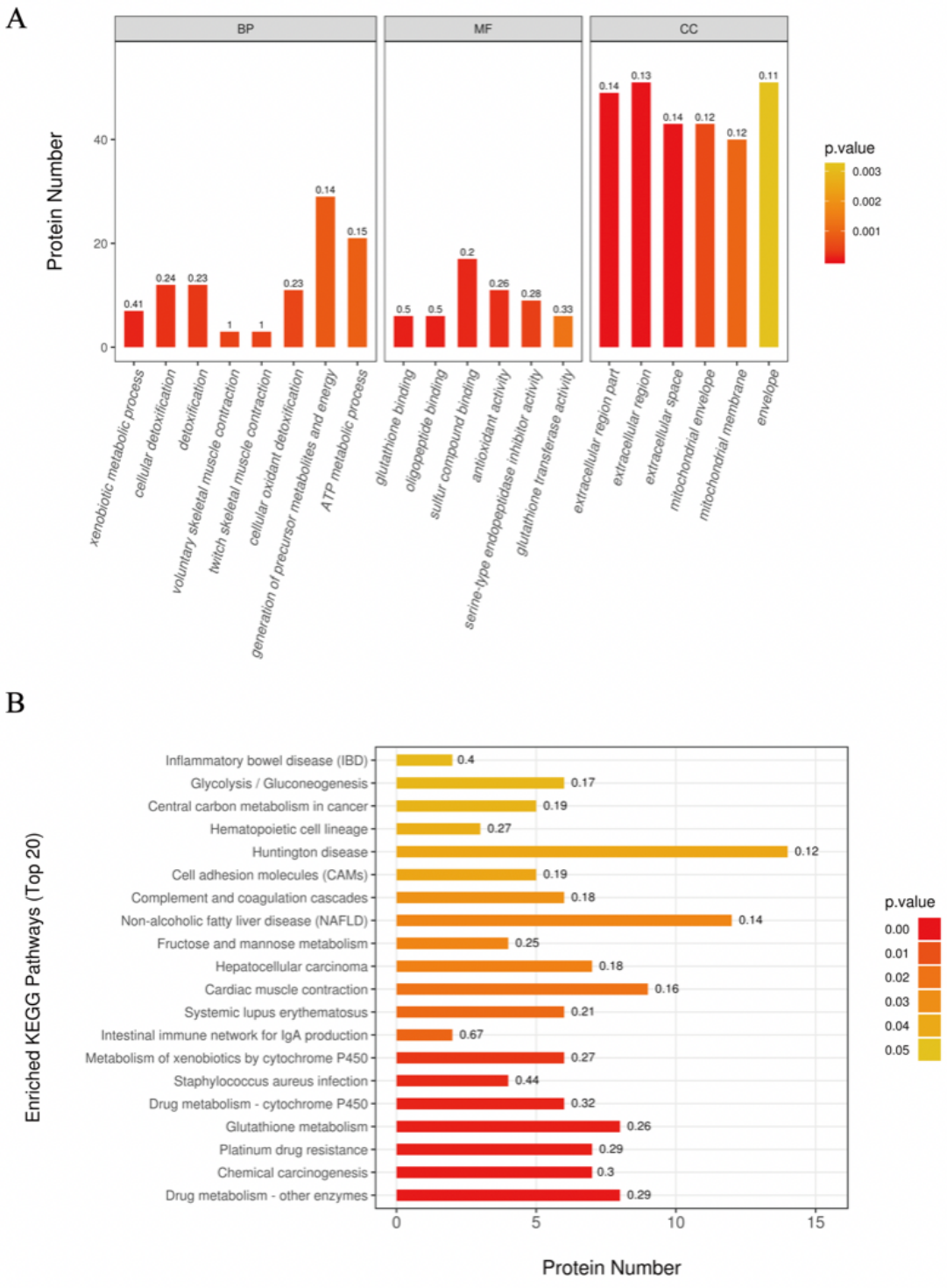


## Figure 3

Differentially expressed proteins pathway enrichment analysis. (A) The most significantly ($p < 0.05$) enriched GO terms (Top 20) in rat treated with doxorubicin. (B) The most significantly ($p < 0.05$) enriched KEGG pathways (Top 20) in rat treated with doxorubicin. (BP: biological process; MF: molecular function; CC: cellular component).

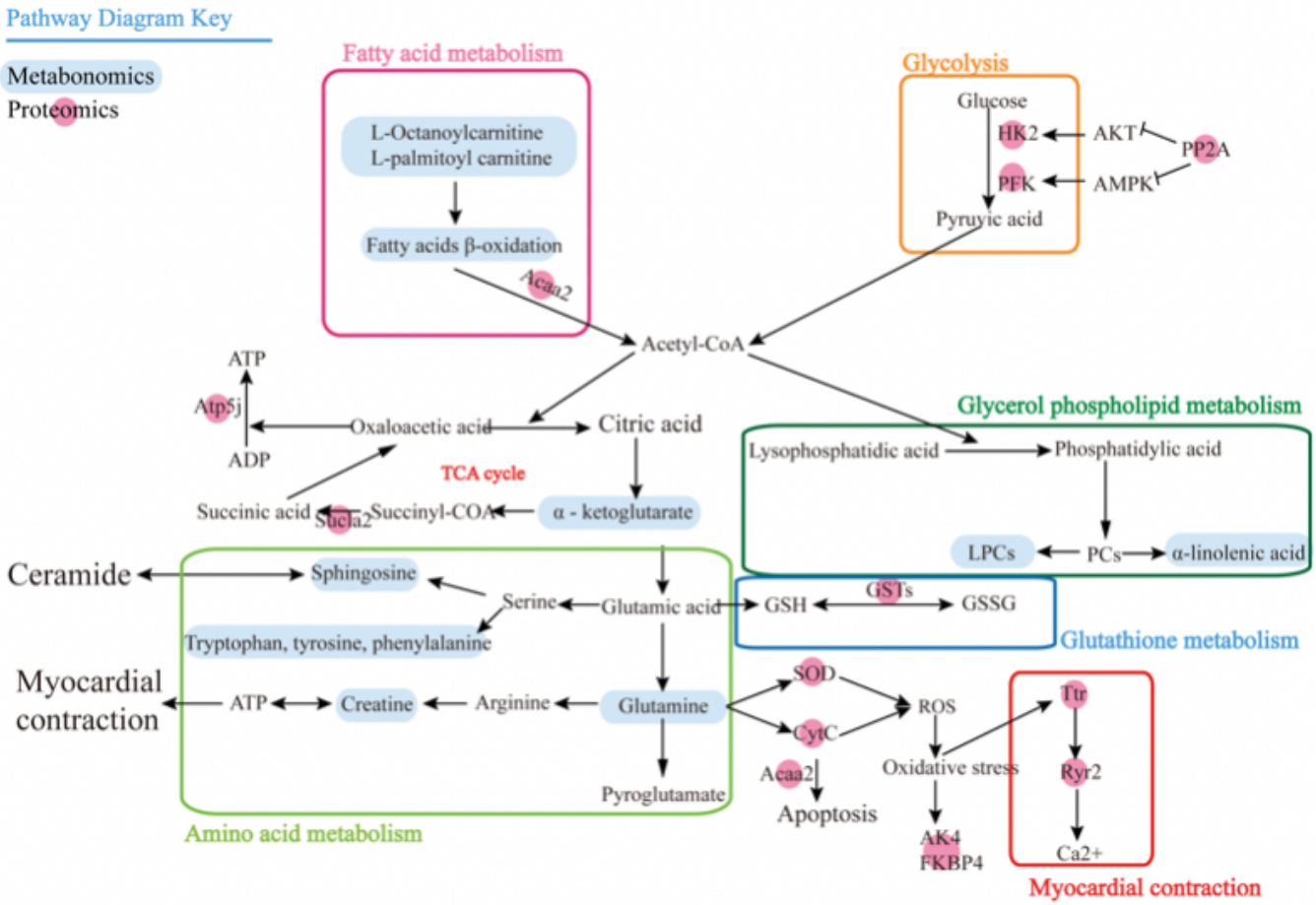


## Figure 4

Pathway map for combined analysis of metabolomics and proteomics.

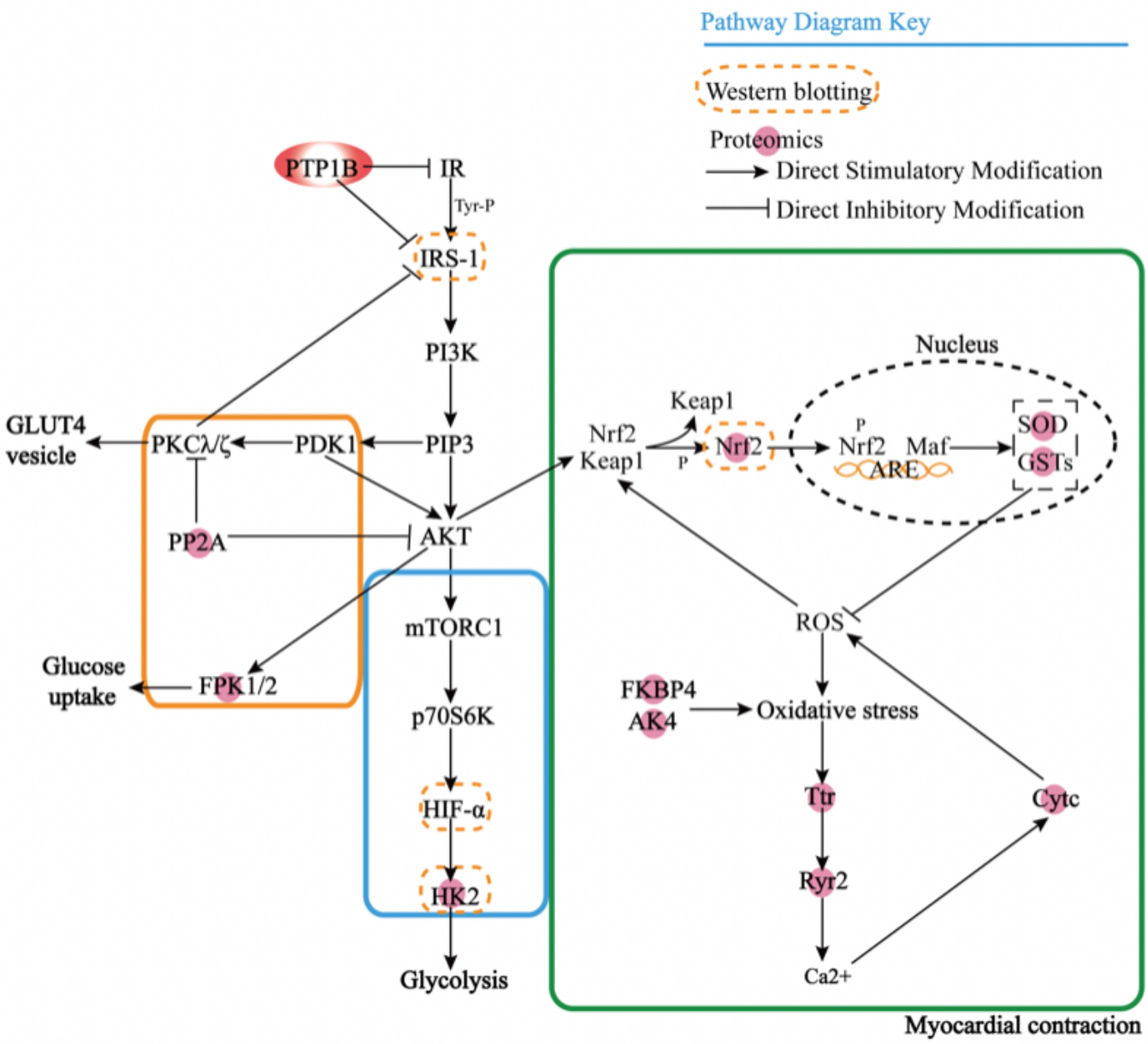


## Figure 5

Interaction mechanism between PTP1B and differential proteins.

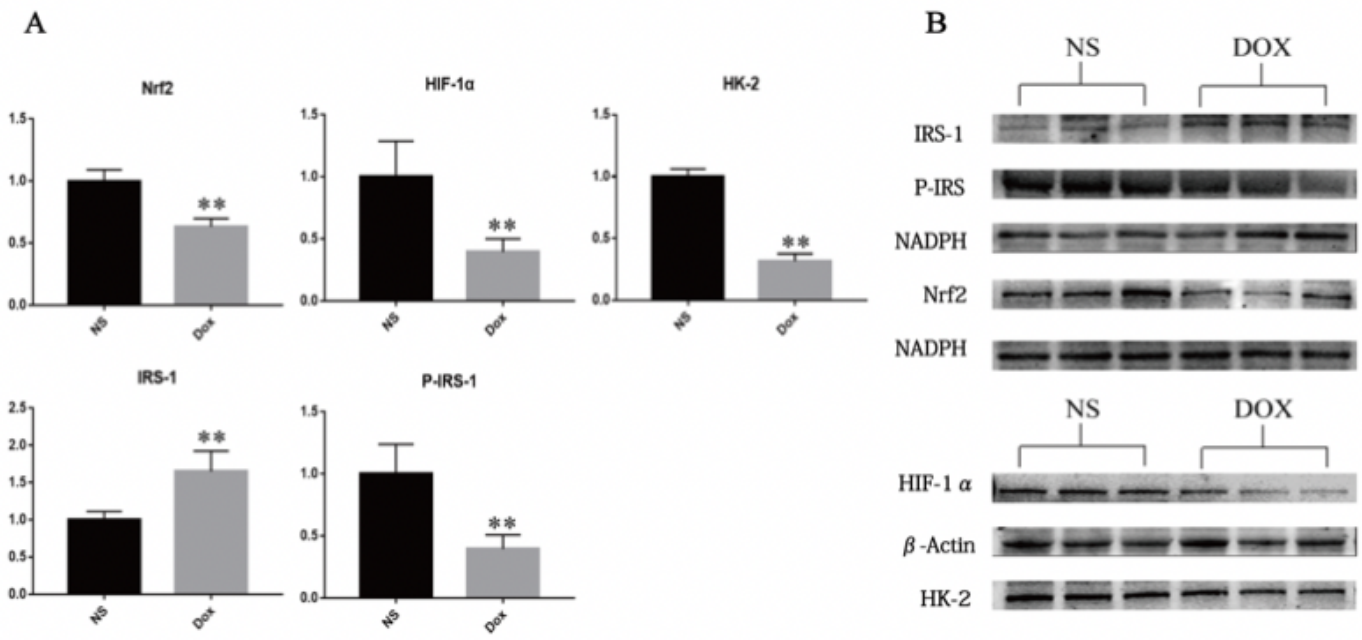


**Figure 6**

The expression of NS and DOX related proteins in heart tissue(*p < 0.05; **p < 0.01). (A) Expression level of Nrf2, HIF−1α, HK−2, IRS−1, P−IRS in NS group and DOX group. (B) Protein level of Nrf2, HIF−1α, HK−2, IRS−1, P−IRS in NS group and DOX group.

# Supplementary Files

This is a list of supplementary files associated with this preprint. Click to download.

- Supplementary1.docx
- Supplementary2.xlsx